[CANCER RESEARCH 63, 4960–4966, August 15, 2003]

Effects of Overexpression of Dimethylarginine Dimethylaminohydrolase on Tumor Angiogenesis Assessed by Susceptibility Magnetic Resonance Imaging[1]

Vassiliki Kostourou,[2] Simon P. Robinson,[3] Guy St. J. Whitley, and John R. Griffiths

Department of Basic Medical Sciences, St. George's Hospital Medical School, London SW17 ORE, United Kingdom

ABSTRACT

Intracellular factors that regulate nitric oxide (NO) synthesis represent important targets in tumor progression. Overexpression of dimethylarginine dimethylaminohydrolase (DDAH), which metabolizes the endogenous inhibitors of NO synthesis asymmetric dimethylarginine and *N*-monomethyl-L-arginine, results in C6 gliomas with enhanced growth rate compared with wild type. To investigate the effects of DDAH on tumor vascular morphogenesis *in vivo*, we have measured the transverse relaxation rates R_2* and R_2 in clone D27 gliomas overexpressing DDAH and C6 wild-type gliomas using intrinsic susceptibility magnetic resonance imaging (MRI), sensitive to changes in endogenous [deoxyhemoglobin], and susceptibility contrast-enhanced MRI using the intravascular blood pool contrast agent NC100150, and we compared the results with fluorescence microscopy of the tumor uptake of the perfusion marker Hoechst 33342. The baseline R_2* was significantly faster in the D27 tumors, consistent with a greater vascular development ($P < 0.02$, ANOVA). There was no significant difference between the response of the two tumor types to hypercapnia (5% CO_2/95% air), used as a probe for vascular maturation, or hyperoxia (5% CO_2/95% O_2), used as a probe for vascular function. NC100150 increased the R_2* and R_2 rates of both tumor types and demonstrated a significantly larger blood volume in the D27 tumors ($P < 0.02$, ANOVA). This correlated with a significantly greater uptake of Hoechst 33342 in the D27 tumors compared with C6 wild-type tumors ($P < 0.02$, ANOVA). Despite the increased tumor blood volume, the ΔR_2*/ΔR_2 ratio, an index of microvessel size, showed that the capillaries in the two tumor types were of a similar caliber. The data highlight the potential of susceptibility MRI-derived quantitative end points to noninvasively assess tumor angiogenesis, and in this regard, the use of intravascular blood pool contrast agents such as NC100150 appears very promising. Overexpression of DDAH results in increased neovascularization of C6 gliomas *in vivo*. The lack of significant difference in hypercapnic/hyperoxic response between the C6 and D27 tumors and the similar vessel caliber are also consistent with a role for DDAH in the initial stages of vasculogenesis.

INTRODUCTION

Angiogenesis is the development of new blood vessels to provide a nutritive blood supply and is a prerequisite for tumor growth and survival (1). Tumor blood vessels can grow by sprouting, intussusception, or the incorporation of endothelial cell precursors. Angiogenesis is stimulated by the release of specific growth factors from tumor cells, endothelial cells, or associated macrophages, in particular VEGF[4] (2). Production of these factors is up-regulated by physiological conditions associated with tumors, *e.g.*, hypoxia, low glucose, and pH, all of which are consistent with a compromised blood supply.

Numerous angiogenic stimuli also induce the production of NO, and strong positive correlations between nitric oxide synthase expression and human tumor grade have been demonstrated (3–7). Intracellular factors that regulate NO synthesis may therefore represent important targets in the control of tumor growth. We recently showed that C6 glioma cells genetically engineered to constitutively overexpress the enzyme DDAH resulted in tumors that grew twice as fast as the wild type (8). DDAH metabolizes two competitive inhibitors of NO synthesis, asymmetric dimethylarginine and *N*-monomethyl-L-arginine, indirectly leading to an increase in NO production. Inhibition of DDAH activity leads to decreased NO production both *in vitro* and *in vivo* (9). Upon excision, tumors derived from C6 cells overexpressing DDAH bled more profusely compared with wild type. Subsequent analysis showed increased expression and secretion of VEGF in tumors overexpressing DDAH (8).

^{1}H MRI, with its high temporal and spatial resolution, presents itself as an ideal technique as a noninvasive assay of tumor angiogenesis *in vivo* (10, 11). In particular, two complementary magnetic susceptibility-based MRI approaches have been used in this regard. Firstly, tumor vasculature has been detected using the intrinsic R_2* contrast produced by paramagnetic deoxyhemoglobin within tumor blood vessels, to which gradient-recalled echo MRI sequences are sensitive (12). This approach, which is truly noninvasive because it relies on endogenous deoxyhemoglobin for contrast, offers an extremely sensitive method of monitoring the dynamics of vascular modeling, function, and regression *in vivo* (13–16). Secondly, tumor blood volume has been assessed using susceptibility contrast MRI measurements, in which the tumor uptake of USPIO particles is measured. These novel blood pool contrast agents act in a similar way to deoxyhemoglobin but are more powerful in creating susceptibility effects that strongly and locally alter the transverse relaxation rates R_2 and R_2* (17, 18). Contrary to the conventional contrast agent gadopentetate dimeglumine, these high molecular weight USPIO blood pool contrast agents do not leak as readily from the blood vessels. The resulting long intravascular half-life thus simplifies measurements of tumor R_2 and R_2* during steady-state concentrations of the USPIO particles. We have recently shown that estimates of tumor blood volume, derived from measurements of the absolute changes in the relaxation rates R_2 and R_2* after administration of the USPIO blood pool contrast agent NC100150 (Clariscan; Amersham Health), correlate with the tumor blood volume determined by fluorescence microscopy (19). Furthermore, the ratio of relaxivities, ΔR_2*/ΔR_2, can be used to derive maps of capillary diameter (19–22) and has shown good agreement with histologically determined vessel size (20).

To validate MRI-derived end points, it is essential that appropriate histological analyses of the tumor vasculature are performed (10). A number of immunohistochemical techniques are available to assess tumor vasculature at a microscopic level, detailed information that is not obtainable by noninvasive, volume-averaging MRI techniques (23–24). One such approach is following the tumor uptake of the perfusion marker Hoechst 33342, from which quantitative histologically derived morphometric parameters of tumors have been deter-

Received 12/23/02; revised 5/7/03; accepted 6/10/03.

The costs of publication of this article were defrayed in part by the payment of page charges. This article must therefore be hereby marked *advertisement* in accordance with 18 U.S.C. Section 1734 solely to indicate this fact.

[1] Supported by Cancer Research UK (CRC) Grant C12/A1209, St. George's Hospital Medical School, and The Royal Society. S. P. R. is the recipient of a Royal Society University Research Fellowship.

[2] Present address: Vascular Development Laboratory, Cancer Research UK, London Research Institute, 44 Lincoln's Inn Fields, London WC2A 3PX, United Kingdom.

[3] To whom requests for reprints should be addressed, at Department of Basic Medical Sciences, St. George's Hospital Medical School, Cranmer Terrace, London SW17 ORE, United Kingdom. Phone: 0208-266-6421; Fax: 0208-725-2992; E-mail: s.robinson@sghms.ac.uk.

[4] The abbreviations used are: NO, nitric oxide; VEGF, vascular endothelial growth factor; DDAH, dimethylarginine dimethylaminohydrolase; MRI, magnetic resonance imaging; MGRE, multigradient recalled echo; USPIO, ultrasmall superparamagnetic iron oxide; TE, echo time; SI, signal intensity; ROI, region of interest.

mined and correlated with noninvasive MRI studies of physiological processes (19, 25).

To assess the effects of overexpression of DDAH on tumor angiogenesis, we used both intrinsic susceptibility and susceptibility contrast MRI to assess the tumor vascular architecture and morphology *in vivo* of tumors derived from C6 glioma cells that constitutively overexpress DDAH and tumors derived from wild-type C6 cells. In addition, fluorescence microscopy of tumor uptake of Hoechst 33342 was quantified to assess the perfused fraction of the tumor.

MATERIALS AND METHODS

Animals and Tumors. Wild-type C6 cells and clone 27 (D27) C6 glioma cells, transfected with the full coding region of the rat *DDAH I* gene, were used (8). Cells (2×10^6) were injected into the flanks of female *nu/nu* mice under halothane anesthesia. Because tumors derived from mock-transfected cells grew similarly to wild type *in vivo* (8), MRI was performed only on C6 wild-type and D27 tumors. Two separate cohorts of each tumor type were used for intrinsic susceptibility and susceptibility contrast MRI. All experiments were performed in accordance with the United Kingdom Home Office Animals Scientific Procedures Act 1986.

MRI. Size-matched C6 wild-type (mean volume, 1.05 ± 0.2 cm^3) and D27 (mean volume, 1.06 ± 0.2 cm^3) tumors were imaged at 23 and 18 days postpassage, respectively. Anesthesia was induced with a 10 ml/kg i.p. injection of fentanyl citrate (0.315 mg/ml) plus fluanisone [10 mg/ml (Hypnorm; Janssen Pharmaceutical Ltd.)], midazolam [5 mg/ml (Hypnovel; Roche)], and water (1:1:2). ^{1}H MRI was performed on a Varian 4.7T instrument using a two-turn 12-mm coil. The anesthetized animals were positioned so the tumor hung vertically into the radiofrequency coil and covered with a warm water blanket to maintain the core temperature at 37°C. Field homogeneity was optimized by shimming on the water signal for each tumor to a linewidth of 30–40 Hz.

Tumor vascular development, maturation, and function were assessed by MGRE MRI (26, 27). Images with increasing T_2* weighting were acquired using a gradient echo sequence with TE = 5 to 40 ms, echo spacing of 5 ms, 8 echoes, repetition time = 100 ms, and flip angle $\alpha = 45°$. Images were acquired from three transverse 1-mm slices through the tumor, using 8 acquisitions of 256 phase encode steps over a 4×3-cm field of view for each TE. The total imaging time was ~9 min. Air, 5% CO_2 in air, or carbogen (5% CO_2/95% O_2) was administered via a nose piece equipped with a scavenger to prevent the leakage of paramagnetic oxygen into the magnet bore, which could potentially change the magnetic susceptibility around the coil and produce image artifacts. MGRE images were first acquired during air breathing, subsequently during 5% CO_2 in air breathing, and finally during carbogen breathing.

Paramagnetic deoxyhemoglobin creates susceptibility perturbations around blood vessels, increasing the magnetic resonance transverse relaxation rate R_2* ($R_2^* = 1/T_2^*$, the apparent spin-spin relaxation time). Sampling the MGRE MRI SI at several TEs allows the slope of ln(SI) *versus* TE to be calculated, which determines R_2* and is directly proportional to the tissue content of deoxyhemoglobin and hence a sensitive index of tissue vascularity. A fast R_2* is consistent with a high [deoxyhemoglobin] and hence indicative of high blood vessel density. In addition, the intercept of the fitted data, *i.e.*, the SI at TE = 0 (A_0), is exclusively sensitive to changes in perfusion. A decrease in the slope (R_2*) implies an increase in oxyhemoglobin. Blood vessel maturation and function were also assessed by measuring the changes in tumor R_2* during hypercapnia (5% CO_2/95% air) as a probe for vascular smooth muscle dilation or during hyperoxia (5% CO_2/95% O_2) to indicate functional blood vessels, respectively (13, 14, 16). Apparent R_2* and A_0 maps were calculated on a pixel-by-pixel basis from the MGRE image data sets (26, 27). The average apparent R_2* relaxation rates were calculated for each tumor for a global ROI encompassing the whole tumor image but excluding the surrounding skin and muscle. A relatively fast R_2* is consistent with a high [deoxyhemoglobin] and hence vascularization, but cellular paramagnetic debris from necrosis such as hemosiderin can also increase R_2*. Therefore, the intercept A_0 maps, which are exclusively sensitive to perfusion, were used to identify local ROIs that showed relatively high SI and hence were vascular, and changes in R_2* within them were subsequently assessed (Fig. 1).

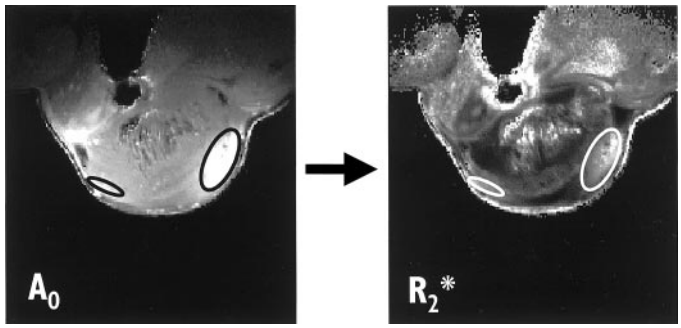

Fig. 1. Calculated A_0 and R_2* maps from one C6 glioma synthesized on a pixel-by-pixel basis from one MGRE MRI data set (23). The A_0 intercept maps, which are exclusively sensitive to perfusion, were used to identify local ROIs (vascular hot spots) that showed relatively high SI as shown, and changes in R_2* within them in response to hypercapnia/hyperoxia were subsequently assessed.

Tumor blood volume was assessed by susceptibility contrast MRI measurements, made from a single central transverse 2-mm-thick slice through the tumor (19). MGRE images were acquired as described above to quantify R_2*. A multispin echo sequence was used to quantify R_2, with repetition time = 300 ms and TE = 11, 20, 30, and 40 ms. Images were acquired from exactly the same 4×3-cm field of view. The total imaging time for a complete set of MGRE and multispin echo images was ~15 min. After acquisition of one set of images, 2.5 mgFe/kg NC100150 [Clariscan; Amersham Health (28, 29)] was administered via a tail vein, and two additional sets of images were acquired. Apparent R_2 and R_2* maps were calculated on a pixel-by-pixel basis from the image data sets as described above to quantify tumor R_2 and R_2*. Spin echo MRI techniques have a lower sensitivity compared with gradient echo; hence, the increase in R_2 induced by a susceptibility contrast agent is smaller than the increase in R_2*. However, spin echoes are relatively insensitive to deoxyhemoglobin-induced macroscopic susceptibility gradients and erythrocyte blood flow (which are essentially artifactual), to which gradient echoes are highly sensitive. Therefore, changes in R_2 reflect the capillary microvasculature, making them useful in depicting functional/physiological vascular changes, *e.g.*, angiogenesis, whereas R_2* is sensitive to both micro- and macrovasculature (17, 18, 20). Tumor vascular morphology was also assessed by first deriving maps of ΔR_2* and ΔR_2, the differences between the relaxation rates before and after injection of NC100150. From these, the ratio map of $\Delta R_2^*/\Delta R_2$ was derived. The ratio $\Delta R_2^*/\Delta R_2$ increases with increasing vessel size and was thus used as an index of the average microvessel size over the whole tumor (19, 20, 22).

Fluorescence Microscopy of a Perfusion Marker. Tumor-bearing mice received i.v. injection via a tail vein of 15 mg/kg of the perfusion marker Hoechst 33342 in PBS (19, 23, 24). Hoechst 33342 stains the nuclei of endothelial cells and cells adjacent to tumor blood vessels that are perfused at the time of i.v. injection and hence delineates functional tumor vasculature. One min after injection, the animals were killed by cervical dislocation to prevent the Hoechst dye from diffusing too far from perfused vessels, and the tumors were excised rapidly, frozen, and stored in liquid nitrogen. Frozen sections (10 μm) were subsequently cut. Fluorescence signals of whole tumor sections were recorded using a motorized scanning stage (Marzhauser) driven by Stage-Pro (Media Cybernetics) on an IX70 fluorescence microscope (Olympus Optical Co. Ltd.). Digital images from both C6 and D27 tumors were acquired using the same exposure time, and composite images were then synthesized from each field using Image-Pro Plus software (Media Cybernetics). Fluorescent particles were detected above a threshold that was constant for all of the composite images (analySIS; Soft Imaging System), and the area of the tumor section with Hoechst 33342 fluorescence was then determined and expressed as a percentage of the whole tumor section (mean perfused area). Because the images were acquired and analyzed under identical conditions, any differences in the mean perfused area would result from differences in tumor perfusion.

RESULTS

Synthesized A_0 and R_2* maps obtained from one C6 wild-type and one D27 tumor while the host breathed air, 5% CO_2/95% air, and,

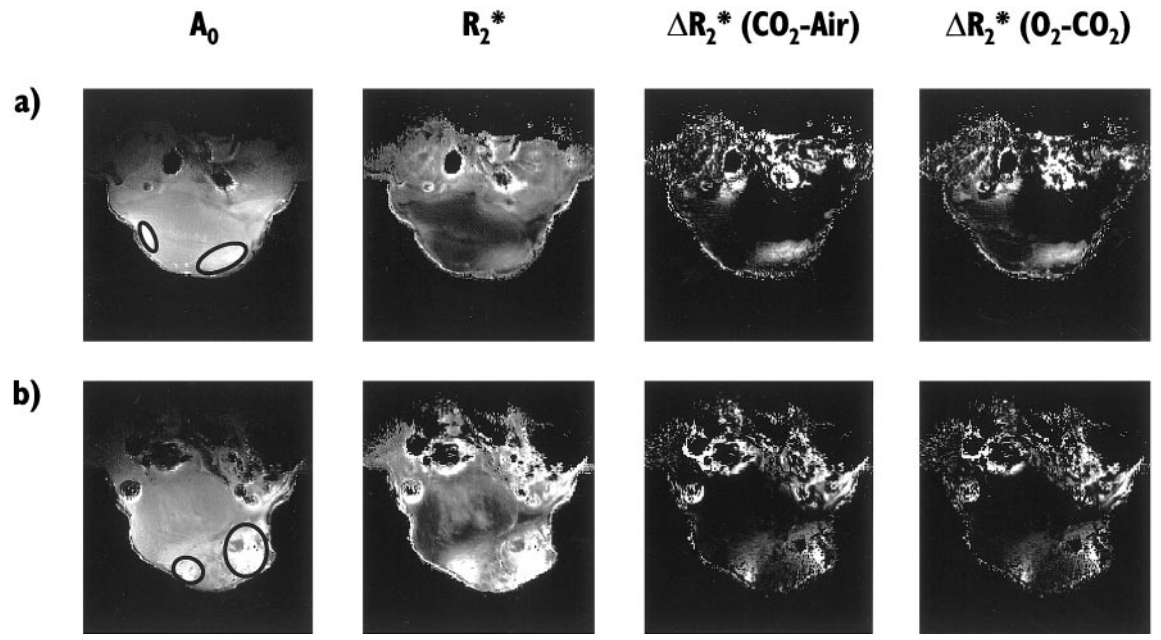

Fig. 2. Calculated A_0 and R_2* maps obtained from (*a*) a C6 wild-type tumor and (*b*) a D27 tumor while the host breathed air, and the difference (ΔR_2*) maps obtained in response to challenge with hypercapnia (5% CO_2/95% air) and hyperoxia (5% CO_2/95% O_2). The greater SI over the baseline R_2* map of the D27 tumor is consistent with a greater (deoxyhemoglobin) and hence vascular development. The local ROIs showing relatively high SI and thus used to investigate localized changes in R_2* in response to hypercapnia/hyperoxia are highlighted on the perfusion-sensitive A_0 intercept maps.

finally, 5% CO_2/95% O_2 are shown in Fig. 2. Overall, both D27 and wild-type tumors exhibited heterogeneity in the R_2* maps, with regions of both high and low SI identified within the tumor. Tumors derived from D27-transfected cells were more vascularized compared with tumors derived from wild-type cells, as indicated by the significantly faster average baseline R_2* shown in Fig. 3. No significant change in tumor R_2* over the whole tumor could be detected in either of the tumor lines in response to 5% CO_2/95% air or 5% CO_2/95% O_2. In an approach analogous to histological vascular hot spot analysis, local ROIs showing relatively high SI in the perfusion-sensitive A_0 intercept maps were identified and were predominantly found within the rim of the tumor (Figs. 1 and 2). The baseline R_2* measured from these local ROIs was also significantly faster in the D27 tumors compared with C6 wild type. Small decreases in R_2* were measured from these vascular hot spots in both tumor lines during hypercapnia and hyperoxia (Fig. 3).

Synthesized R_2 and R_2* maps from one C6 wild-type tumor and one D27 tumor before administration of 2.5 mgFe/kg NC100150 and the ΔR_2 and ΔR_2* maps acquired in the presence of the USPIO particles are shown in Fig. 4. Again, both C6 wild-type and D27 tumors exhibited heterogeneity in the R_2* maps both before and after administration of the blood pool agent, whereas the R_2 maps were more homogeneous. The baseline R_2* and R_2 and the changes induced by NC100150 are shown in Fig. 5. There was no significant difference between the average R_2* of the two cohorts of each tumor type used in this study and those in the MGRE MRI experiments. As before, the average baseline R_2* measured over the whole tumor was significantly faster in the D27 tumors than in the C6 wild-type tumors. NC100150 induced significant increases in both R_2* and R_2 of both C6 wild-type and D27 tumors, and this response was significantly greater in the D27 tumors. This response was sustained in the second set of images acquired after administration of NC100150, suggesting negligible leakage of NC100150 out of the tumor vasculature over the 30-min time period (data not shown).

Tumor vascular morphology was also assessed by deriving maps of the ΔR_2*/ΔR_2 ratio, a ratio that increases with increasing microvessel size. Fig. 6 shows calculated ΔR_2*/ΔR_2 maps of the same tumors in Fig. 4. The intensity of the synthesized ΔR_2*/ΔR_2 maps of both C6 and D27 tumors is similar. The average ΔR_2*/ΔR_2 ratio for both C6 and D27 tumors is also summarized in Fig. 6*c*, and there was no significant difference between the two tumor types.

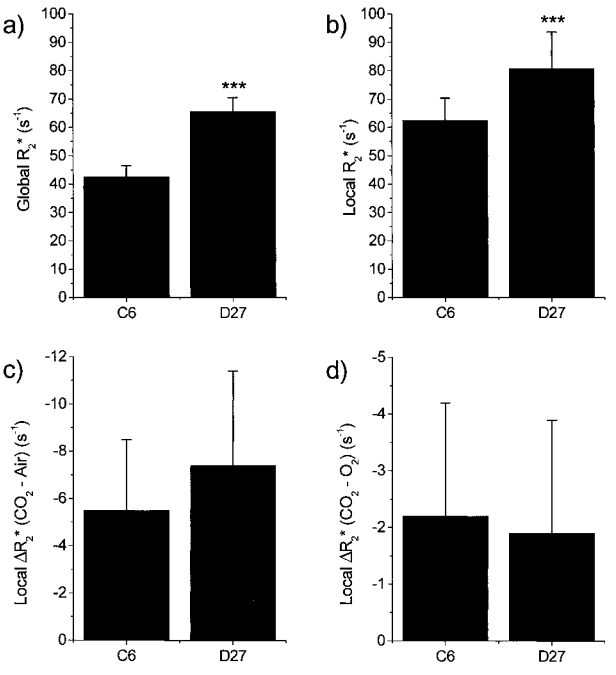

Fig. 3. Average baseline R_2* (mean ± 1 SE; $n = 8$) measured over the whole tumor and from localized regions and changes in R_2* within the same local regions, in response to hypercapnia and hyperoxia, determined by MGRE MRI for wild-type C6 and clone D27 gliomas. The average baseline R_2* measured (*a*) over the whole tumor and (*b*) from local ROIs was significantly faster in the D27 tumors than in the C6 wild-type tumors (***, $P < 0.01$, ANOVA). No significant changes in tumor R_2* were found in response to challenge with (*c*) 5% CO_2 in air or (*d*) 5% CO_2/95% O_2 over the whole tumor. Nevertheless, small decreases in R_2* were measured from local ROIs in both tumor lines during hypercapnia and hyperoxia.

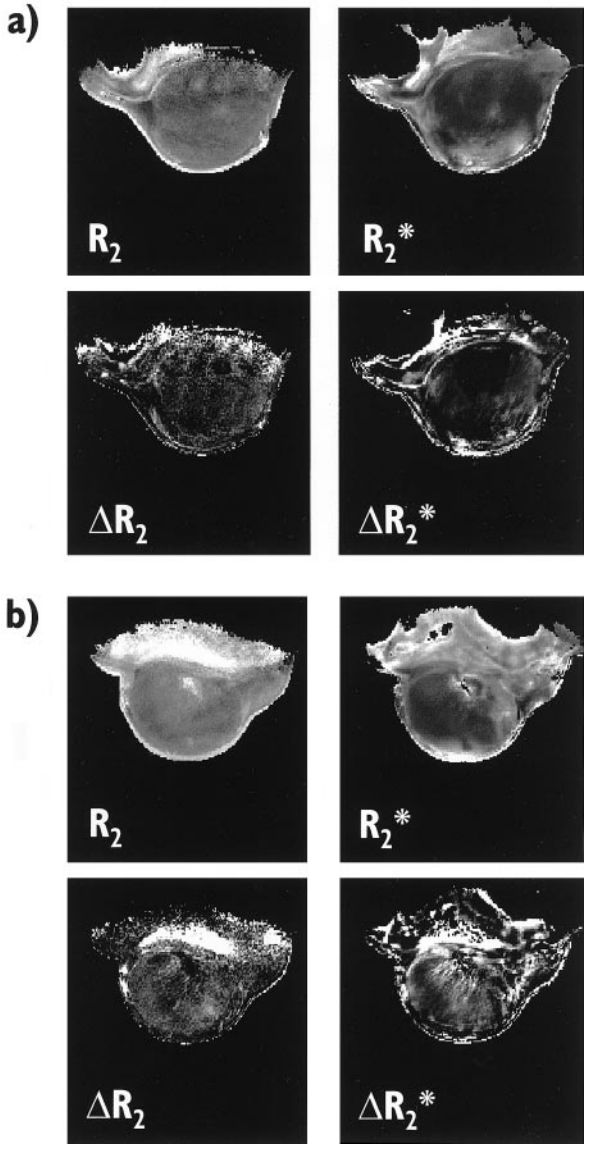

Fig. 4. Calculated R_2 and R_2* maps from (*a*) a C6 wild-type tumor and (*b*) a D27 tumor before administration of 2.5 mgFe/kg NC100150 and the ΔR_2 and ΔR_2* maps acquired in the presence of the USPIO particles. Both tumor types showed an increase in relaxation rates after administration of the blood pool agent, and this increase was significantly greater in the D27 tumors.

Analysis of the tumor perfusion was performed on sections obtained from mice treated with Hoechst 33342. Fig. 7 shows composite fluorescence microscopy images of the perfused vascular architecture obtained from one C6 wild-type tumor and one D27 glioma. A greater abundance of Hoechst 33342 staining was associated with the D27 tumors, consistent with the D27 tumors having more perfused vessels. The mean perfused areas obtained for the two tumor types are summarized in Fig. 7*c*, which shows that the perfusion of the D27 tumors was significantly greater than that of the C6 wild-type tumors.

DISCUSSION

Investigation of tumor angiogenesis *in vivo* within genetically manipulated tumors expressing a well-defined phenotypic change gives an opportunity to investigate the role of factors implicated in tumor vascular morphogenesis *in vivo* and the chance to identify, validate, and calibrate MRI-derived prognostic and diagnostic indices that can be translated into the clinic (13, 14, 16, 30). We have used this powerful approach to evaluate the effects of DDAH on tumor angiogenesis *in vivo*.

MGRE MRI permits efficient, quantitative assessment of the role of factors implicated in tumor blood vessel development. Image contrast arises only from intravascular RBCs, and contrast changes are not sensitive to vascular permeability. The significantly faster baseline R_2* of the D27 tumors is consistent with these more rapidly growing D27 gliomas having a greater vascular development (*i.e.*, angiogenesis) compared with wild-type C6 gliomas (8).

The maturation state of tumor vasculature has recently been suggested as a marker of tumor progression, with the recruitment of pericytes resulting in tumor blood vessels refractory to withdrawal of vascular growth factors such as VEGF (13, 14). Clinical measures of capillary maturation may thus assist the identification of patients who would benefit from antiangiogenic therapies or vascular targeting treatments (31–33). In this study, the maturation and functional state of the tumor blood vessels were probed by measuring the ΔR_2* in response to hypercapnia and hyperoxia, respectively. Small decreases in R_2* were identified within the periphery of tumors derived from both wild-type C6 and D27 cells, presumably indicating areas of active angiogenesis. These results are consistent with the blood vessels of both tumor types containing (*a*) some smooth muscle in the vessel walls and (*b*) deoxygenated blood. There was no significant difference in either response between the C6 and D27 gliomas.

Administration of 2.5 mgFe/kg NC100150 was a sufficient dose at 4.7 Tesla to induce significant changes in the transverse relaxation rates R_2* and R_2 of both wild-type C6 and D27 gliomas, and this response was heterogeneous over the whole tumor. There was no

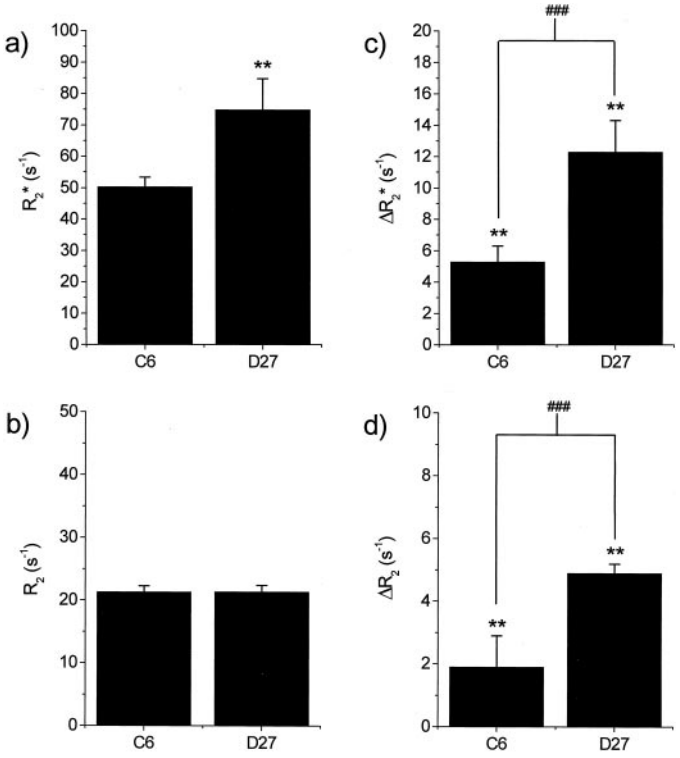

Fig. 5. Average baseline (*a*) R_2* and (*c*) R_2 (mean ± 1 SE) measured over the whole tumor and changes in (*b*) R_2* and (*d*) R_2 after administration of 2.5 mgFe/kg NC100150 measured in wild-type C6 tumors ($n = 6$) and clone D27 gliomas ($n = 5$). There was no significant difference between the average R_2* of the two cohorts of each tumor type used in this study and those in the intrinsic susceptibility MRI experiments (Fig. 3). As before, the average baseline R_2* measured over the whole tumor was significantly faster in the D27 tumors than in the C6 wild-type tumors (**, $P < 0.02$, ANOVA). NC100150 induced significant increases in both R_2* and R_2 of both D27 and wild-type tumors (**, $P < 0.02$, Student's *t* test), and this response was significantly greater in the D27 tumors (###, $P < 0.01$, ANOVA).

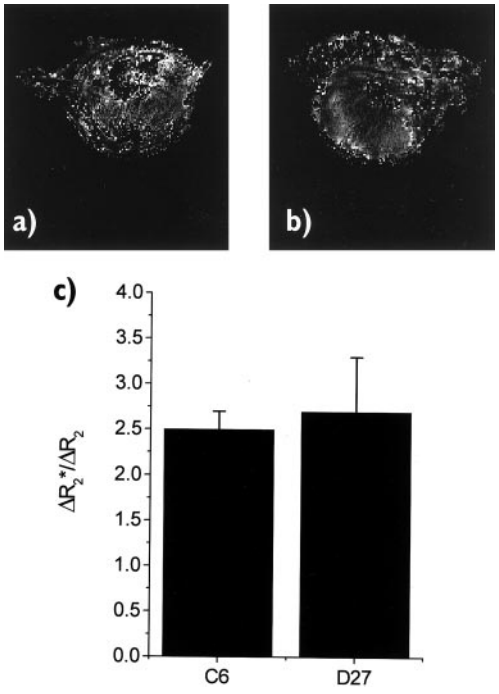

Fig. 6. Calculated $\Delta R_2^*/\Delta R_2$ maps derived from (*a*) the C6 and (*b*) the D27 tumor shown in Fig. 4. *c*, there was no significant difference in the $\Delta R_2^*/\Delta R_2$ ratio between the two tumor types ($P > 0.1$, ANOVA).

apparent recovery to baseline values of either R_2^* and R_2 within the 30 min after the administration of NC100150, implying negligible permeability of NC100150 from the tumor circulation. The significantly larger changes in R_2^* and R_2 measured in the D27 tumors are consistent with a larger blood volume compared with C6 wild type. This was supported by tumor uptake of Hoechst 33342, which showed that the perfused area in the D27 tumors was significantly greater than that in the C6 wild-type tumors (Fig. 7) and confirmed our earlier observations (8). These data highlight the advantages of using histological techniques such as Hoechst 33342 that assay for perfused functional vasculature. These methods appear to correlate with angiogenic potential, whereas with blood vessel density measurements using pan-endothelial markers, the correlation with angiogenesis can be unclear (34). The increased blood volume of the D27 tumors is consistent with clinical observations, in which high-grade human gliomas had a substantially higher relative blood volume compared with low-grade tumors (35).

Evaluation of the $\Delta R_2^*/\Delta R_2$ ratio, an index of the average microvessel size, showed no significant differences between the D27 and wild-type C6 gliomas (Fig. 6). This implies that, despite the clearly increased tumor blood volume in the D27 tumors, the caliber of the vasculature in the two tumor types is similar. Using the methodology of Tropres *et al.* (22), we have recently shown that estimates of both the tumor fractional blood volume and microvessel size could be calculated using the NC100150-induced changes in R_2^* and the $\Delta R_2^*/\Delta R_2$ ratio, respectively (19). Assuming that the susceptibility change induced by NC100150 was the same for both tumor types, and using a previously reported diffusion coefficient for C6 gliomas of 1.1×10^{-9} $m^2 s^{-1}$ (36), the fractional blood volume of the D27 and C6 gliomas was estimated to be 3% and 1%, respectively, whereas the average microvessel size for both tumor types was 6 μm. This is not dissimilar from previous histological measurements (mean $\pm$ 1 SE) of the microvessel diameter of C6 gliomas of 7.8 $\pm$ 0.5 μm (37) and 12.5 $\pm$ 3.9 μm (20).

Taken together, the results are consistent with enhanced tumor

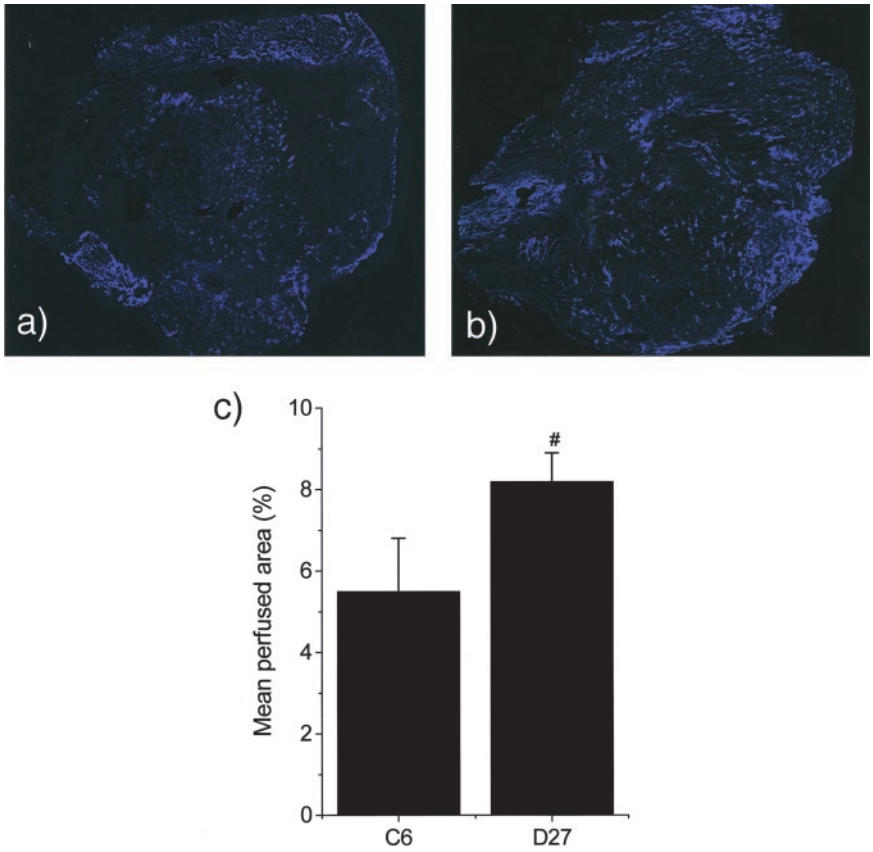

Fig. 7. Representative composite fluorescence microscopy images of the perfused vascular architecture obtained from (*a*) a C6 tumor and (*b*) a D27 glioma after administration of the perfusion marker Hoechst 33342. Because Hoechst 33342 was only allowed to circulate for 1 min, it only stained the nuclei of endothelial cells and cells adjacent to tumor blood vessels that were perfused at the time of i.v. injection and hence delineates functional tumor vasculature. *c*, a greater abundance of Hoechst 33342 staining was associated with the D27 tumors, and the mean perfused fraction of the D27 tumors ($n = 6$) was significantly greater than that of C6 wild-type tumors ($n = 5$; #, $P < 0.05$, ANOVA).

angiogenesis in D27 tumors and suggest that DDAH activity might play a central role in tumor growth by regulating the concentration of tumor-derived NO. The spatial and temporal production of NO is tightly regulated and could be an important factor in determining tumor progression. We have previously shown enhanced VEGF production by D27 tumors compared with C6 wild-type tumors, suggesting that DDAH may enhance tumor growth and angiogenesis via VEGF expression (8). The lack of significant difference in (*a*) the hypercapnic/hyperoxic response and (*b*) vessel caliber between the C6 and D27 tumors suggests that DDAH is primarily involved in the initial formation of tumor blood vessels, either through angiogenic sprouting or intussusception, rather than the subsequent stages of vascular remodeling (1). Support for this has come from *in vitro* invasion assays reported previously (8).

Intrinsic susceptibility-based MRI measurements were made on a tumor system in which DDAH was *constitutively* overexpressed, and the results were compared with wild type. A similar approach has been used previously to investigate the role of hypoxia-inducible factor 1α in tumor angiogenesis (38). The localized tumor ΔR_2* responses to hypercapnia and hyperoxia measured by MGRE MRI herein were inherently small, a consequence of the reduced contrast: noise ratio of intrinsic contrast-enhanced MRI. Murine erythrocytes in whole blood are typically 6 μm in diameter (19). Thus, the ability of murine erythrocytes, the primary source of changes in R_2* intrinsic contrast, to traverse similarly sized, tortuous capillaries *in vivo* would be limited, abrogating the hypercapnic/hyperoxic response (19). This would explain why, contrary to the hyperoxic ΔR_2* response, a higher proportion of functional vasculature was measured in the D27 tumors after Hoechst 33342 uptake. Susceptibility contrast MRI has been used previously to show an increased blood volume fraction in murine MCF-7 mammary carcinomas constitutively overexpressing VEGF compared with nontransfected controls (30). In this study, we have clearly demonstrated the utility of NC100150 to show that overexpression of DDAH in C6 gliomas resulted in a greater tumor blood volume compared with wild type, yet the sizes of the vessels in the two tumor types were similar. An alternative approach to investigate both the effects and dynamics of DDAH on vascular remodeling assessed by intrinsic susceptibility MRI and the contribution of DDAH to vascular morphology assessed by the microvessel size index ratio ΔR_2*/ΔR_2 after susceptibility contrast MRI would be to use a tumor system in which DDAH is under inducible control, rather than being constitutively overexpressed, and where each tumor acts as its own control. A C6 cell line in which production of DDAH is under the control of a tetracycline-inducible promoter is currently being engineered.

The development and validation of quantitative, clinically applicable MRI end points of functional/physiological measures of tumor angiogenesis is critical for (*a*) enhancing our understanding of the incipient tumor vasculature and (*b*) determining the efficacy of antiangiogenic and antivascular therapies, many of which do not induce a significant growth delay in human tumor xenografts (39). The utility of both MRI methods used herein in the clinic has been demonstrated. Recently, MGRE MRI, which can be implemented on most clinical MRI scanners, was used to measure human tumor R_2* during air and carbogen breathing to assess the prognostic value of ΔR_2* for radiotherapeutic outcome (40). The blood pool agent NC100150 was used recently to measure vessel permeability and blood volume in human breast cancers (41). The methods also present themselves as simpler than dynamic T_1-weighted contrast-enhanced MRI using gadopentetate dimeglumine approaches to employ in the clinic because there is no need for rapid data acquisition, and the data analysis and interpretation are more facile. In particular, noninvasive susceptibility-based MRI incorporating USPIO contrast agents such as NC100150 appears very promising.

In summary, both baseline intrinsic susceptibility (deoxyhemoglobin) and steady-state contrast-enhanced (NC100150) MRI measurements were consistent with increased tumor vascular development and blood volume in the D27 tumors compared to wild-type C6 gliomas. The results are consistent with DDAH having an important role in tumor growth and angiogenesis, particularly in the initial stages of vasculogenesis.

ACKNOWLEDGMENTS

We thank Alan Kidger (Olympus Optical Co. Ltd.) for technical assistance and Chris Brown and his staff for care of the animals.

REFERENCES

1. Carmeliet, P., and Jain, R. K. Angiogenesis in cancer and other diseases. Nature (Lond.), *407:* 249–257, 2000.
2. Yancopoulous, G. D., Davis, S., Gale, N. W., Rudge, J. S., Wiegand, S. J., and Holash, J. Vascular-specific growth factors and blood vessel formation. Nature (Lond.), *407:* 242–248, 2000.
3. Thomsen, L. L., Lawton, F. G., Knowles, R. G., Beesley, J. E., Riveros-Moreno, V., and Moncada, S. Nitric oxide synthase activity in human gynecological cancer. Cancer Res., *54:* 1352–1354, 1994.
4. Cobbs, C. S., Brenman, J. E., Aldape, K. D., Bredt, D. S., and Israel, M. A. Expression of nitric oxide synthase in human central nervous system tumors. Cancer Res., *55:* 727–730, 1995.
5. Thomsen, L. L., Miles, D. W., Happerfield, L., Bobrow, L. G., Knowles, R. G., and Moncada, S. Nitric oxide synthase activity in human breast cancer. Br. J. Cancer, *72:* 41–44, 1995.
6. Gallo, O., Masini, E., Morbidelli, L., Franchi, A., Fini-Storchi, I., Vergari, W. A., and Ziche, M. Role of nitric oxide in angiogenesis and tumor progression in head and neck cancer. J. Natl. Cancer Inst. (Bethesda), *90:* 587–596, 1998.
7. Reveneau, S., Arnould, L., Jolimoy, G., Hilpert, S., Lejeune, P., Saint-Giorgio, V., Belichard, C., and Jeannin, J. F. Nitric oxide synthase in human breast cancer is associated with tumor grade, proliferation rate, and expression of progesterone receptors. Lab. Investig., *79:* 1215–1225, 1999.
8. Kostourou, V., Robinson, S. P., Cartwright, J. E., and Whitley, G. St. J. Dimethylarginine dimethylaminohydrolase I promotes tumour growth and angiogenesis. Br. J. Cancer, *87:* 673–680, 2002.
9. MacAllister, R. J., Parry, H., Kimoto, M., Ogawa, T., Russell, R. J., Hodson, H., Whitley, G. St. J., and Vallance, P. Regulation of nitric oxide synthesis by dimethylarginine dimethylaminohydrolase. Br. J. Pharmacol., *119:* 1533–1540, 1996.
10. Brasch, R. C., Li, K. C. P., Husband, J. E., Keogan, M. T., Neeman, M., Padhani, A. R., Shames, D., and Turetschek, K. *In vivo* monitoring of tumor angiogenesis with MR imaging. Acad. Radiol., *7:* 812–823, 2000.
11. Gillies, R. J., Bhujwalla, Z. M., Evelhoch, J. L., Garwood, M., Neeman, M., Robinson, S. P., Sotak, C. H., and van der Sanden, B. P. J. Applications of magnetic resonance in model systems: tumor biology and physiology. Neoplasia, *2:* 139–151, 2000.
12. Ogawa, S., Lee, T-M., Nayak, A. S., and Glynn, P. Oxygenation-sensitive contrast in magnetic resonance image of rodent brain at high magnetic fields. Magn. Reson. Med., *14:* 68–78, 1990.
13. Abramovitch, R., Frenkiel, D., and Neeman, M. Analysis of subcutaneous angiogenesis by gradient echo magnetic resonance imaging. Magn. Reson. Med., *39:* 813–824, 1998.
14. Abramovitch, R., Dafni, H., Smouha, E., Benjamin, L. E., and Neeman, M. *In vivo* prediction of vascular susceptibility to vascular endothelial growth factor withdrawal: magnetic resonance imaging of C6 rat glioma in nude mice. Cancer Res., *59:* 5012–5016, 1999.
15. Gilead, A., and Neeman, M. Dynamic remodelling of the vascular bed precedes tumor growth: MLS ovarian carcinoma spheroids implanted in nude mice. Neoplasia, *1:* 226–230, 1999.
16. Neeman, M., Dafni, H., Bukhari, O., Braun, R. D., and Dewhirst, M. W. *In vivo* BOLD contrast MRI mapping of subcutaneous vascular function and maturation: validation by intravital microscopy. Magn. Reson. Med., *45:* 887–898, 2001.
17. Boxerman, J. L., Hamberg, L. M., Rosen, B. R., and Weisskoff, R. M. MR contrast due to intravascular magnetic susceptibility perturbations. Magn. Reson. Med., *34:* 555–566, 1995.
18. Barbier, E. L., Lamalle, L., and Decorps, M. Methodology of brain perfusion imaging. J. Magn. Reson. Imaging, *13:* 496–520, 2001.
19. Robinson, S. P., Rijken, P. F. J. W., Howe, F. A., McSheehy, P. M. J., van der Sanden, B. P. J., Heerschap, A., Stubbs, M., van der Kogel, A. J., and Griffiths, J. R. Tumour vascular architecture and function evaluated by non-invasive susceptibility MRI methods and immunohistochemistry. J. Magn. Reson. Imaging, *17:* 445–454, 2003.
20. Dennie, J., Mandeville, J. B., Boxerman, J. L., Packard, S. D., Rosen, B. R., and Weisskoff, R. M. NMR imaging of changes in vascular morphology due to tumor angiogenesis. Magn. Reson. Med., *40:* 793–799, 1998.

21. Le Duc, G., Peoch, M., Remy, C., Charpy, O., Muller, R. N., Le Bas, J. F., and Decorps, M. Use of T_2-weighted susceptibility contrast MRI for mapping the blood volume in the glioma-bearing rat brain. Magn. Reson. Med., *42:* 754–761, 1999.
22. Tropres, I., Grimault, S., Vaeth, A., Grillon, E., Julien, C., Payen, J-F., Lamalle, L., and Decorps, M. Vessel size imaging. Magn. Reson. Med., *45:* 397–408, 2001.
23. Rijken, P. F. J. W., Bernsen, H. J. J. A., and van der Kogel, A. J. Application of an image analysis system to the quantitation of tumor perfusion and vascularity in human glioma xenografts. Microvasc. Res., *50:* 141–153, 1995.
24. Rijken, P. F. J. W., Bernsen, H. J. J. A., Peters, J. P. W., Hodgkiss, R. J., Raleigh, J. A., and van der Kogel, A. J. Spatial relationship between hypoxia and the (perfused) vascular network in a human glioma xenograft: a quantitative multi-parameter analysis. Int. J. Radiat. Oncol. Biol. Phys., *48:* 571–582, 2000.
25. van der Sanden, B. P. J., Rozijn, T. H., Rijken, P. F. J. W., Peters, H. P., Heerschap, A., van der Kogel, A. J., and Bovee, W. M. Noninvasive assessment of the functional neovasculature in 9L-glioma growing in rat brain by dynamic ^{1}H magnetic resonance imaging of gadolinium uptake. J. Cereb. Blood Flow Metab., *20:* 861–870, 2000.
26. Howe, F. A., Robinson, S. P., Rodrigues, L. M., and Griffiths, J. R. Flow and oxygenation dependent (FLOOD) contrast MR imaging to monitor the response of rat tumours to carbogen breathing. Magn. Reson. Imaging, *17:* 1307–1318, 1999.
27. Robinson, S. P., Rodrigues, L. M., Howe, F. A., Stubbs, M., and Griffiths, J. R. Effects of different levels of hypercapnic hyperoxia on tumour R_2* and arterial blood gases. Magn. Reson. Imaging, *19:* 161–166, 2001.
28. Bjornerud, A., Johansson, L. O., and Ahlstrom, H. K. Pre-clinical results with Clariscan (NC100150 Injection); experience with different disease models. Magn. Reson. Mat. Phys. Biol. Med., *12:* 99–103, 2001.
29. Turetschek, K., Huber, S., Floyd, E., Helbich, T., Roberts, T. P. L., Shames, D. M., Tarlo, K. S., Wendland, M. F., and Brasch, R. C. MR imaging characterization of microvessels in experimental breast tumors by using a particulate contrast agent with histopathologic correlation. Radiology, *218:* 562–569, 2001.
30. Lewin, M., Bredow, S., Sergeyev, N., Marecos, E., Bogdanov, A., and Weissleder, R. *In vivo* assessment of vascular endothelial growth factor-induced angiogenesis. Int. J. Cancer, *83:* 798–802, 1999.
31. Benjamin, L. E., Golijanin, D., Itin, A., Pode, D., and Keshet, E. Selective ablation of immature blood vessels in established human tumors follows vascular endothelial growth factor withdrawal. J. Clin. Investig., *103:* 159–165, 1999.
32. Carmeliet, P. Mechanisms of angiogenesis and arteriogenesis. Nat. Med., *6:* 389–395, 2000.
33. Eberhard, A., Kahlert, S., Goede, V., Hemmerlein, B., Plate, K. H., and Augustin, H. G. Heterogeneity of angiogenesis and blood vessel maturation in human tumors: implications for antiangiogenic tumor therapies. Cancer Res., *60:* 1388–1393, 2000.
34. Padhani, A. R., and Husband, J. E. Dynamic contrast-enhanced MRI studies in oncology with an emphasis on quantification, validation and human studies. Clin. Radiol., *56:* 607–620, 2001.
35. Aronen, H. J., Gazit, I. E., Louis, D. N., Buchbinder, B. R., Pardo, F. S., Weisskoff, R. M., Harsh, G. R., Cosgrove, G. R., Halpern, E. F., Hochberg, F. H., and Rosen, B. R. Cerebral blood volume maps of gliomas: comparison with tumor grade and histologic findings. Radiology, *191:* 41–51, 1994.
36. Remy, C., Tropres, I., Peoc'h, M., Farion, R., and Decorps, M. *In vivo* NMR imaging of microvascularization in normal rat brain and in rat brain tumors. *In:* Eighth Annual Meeting of the International Society for Magnetic Resonance in Medicine, p. 100. Berkeley, CA: International Society for Magnetic Resonance in Medicine, 2000.
37. Farrell, C. L., Farell, C. R., Stewart, P. A., Del Maestro, R. F., and Ellis, C. G. The functional microcirculation in a glioma model. Int. J. Radiat. Biol., *60:* 131–137, 1991.
38. Carmeliet, P., Dor, Y., Herbert, J-M., Fukumura, D., Brusselmans, K., Dewerchin, M., Neeman, M., Bono, F., Abramovitch, R., Maxwell, P., Koch, C. J., Ratcliffe, P., Moons, L., Jain, R. K., Collen, D., and Keshet, E. Role of HIF-1α in hypoxia-mediated apoptosis, cell proliferation and tumour angiogenesis. Nature (Lond.), *394:* 485–490, 1998.
39. Cristofanilli, M., Charnsangavej, C., and Hortobagyi, G. N. Angiogenesis modulation in cancer research: novel clinical approaches. Nat. Rev. Drug Discov., *1:* 415–426, 2002.
40. Rijpkema, M., Kaanders, J., Joosten, F., van der Kogel, A., and Heerschap, A. Effects of breathing a hyperoxic hypercapnic gas mixture on blood oxygenation and vascularity of head-and-neck tumors as measured by magnetic resonance imaging. Int. J. Radiat. Oncol. Biol. Phys., *53:* 1185–1191, 2002.
41. Rydland, J., Bjornerud, A., Torheim, G., Kvistad, K. A., and Haraldseth, O. Macromolecular contrast agent for measurement of vessel permeability and blood volume in human breast cancer: first experience. *In:* Tenth Annual Meeting of the International Society for Magnetic Resonance in Medicine, p. 665. Berkeley, CA: International Society for Magnetic Resonance in Medicine, 2002.